

A dynamically deformable microfilter for selective separation of specific substances in microfluidics

EP

Cite as: Biomicrofluidics 14, 064113 (2020); doi: 10.1063/5.0025927

Submitted: 22 August 2020 · Accepted: 4 November 2020 ·

Published Online: 24 December 2020



View Online



Export Citation



CrossMark

Seitaro Kumamoto,^{1,2,a)} Kenshiro Nakatake,¹ Souichiro Fukuyama,¹ Keiichiro Yasuda,² Yusuke Kitamura,³ Masaaki Iwatsuki,⁴ Hideo Baba,⁴ Toshihiro Ihara,³ Yoshitaka Nakanishi,^{3,5} and Yuta Nakashima^{3,5,6,b)}

AFFILIATIONS

¹Graduate School of Science and Technology, Kumamoto University, 2-39-1 Kurokami, Chuo-ku, Kumamoto 860-8555, Japan

²Ogic Technologies Co. Ltd., 2-9-9, Kamikumamoto, Nishi-ku, Kumamoto 860-0079, Japan

³Faculty of Advanced Science and Technology, Kumamoto University, 2-39-1 Kurokami, Chuo-ku, Kumamoto 860-8555, Japan

⁴Faculty of Life Science, Kumamoto University, 1-1 Honjo, Chuo-ku, Kumamoto 860-8556, Japan

⁵Institute of Industrial Nanomaterials, Kumamoto University, 2-39-1 Kurokami, Chuo-ku, Kumamoto 860-8555, Japan

⁶International Research Organization for Advanced Science and Technology, Kumamoto University, 2-39-1 Kurokami, Chuo-ku, Kumamoto 860-8555, Japan

^{a)}Email: s.kumamoto@ogic.ne.jp

^{b)}Author to whom correspondence should be addressed: yuta-n@mech.kumamoto-u.ac.jp. Tel./Fax: +81-96-342-3743

ABSTRACT

To study an environmental or biological solution, it is essential to separate its constituents. In this study, a 3D-deformable dynamic microfilter was developed to selectively separate the target substance from a solution. This microfilter is a fine metallic nickel structure fabricated using photolithography and electroplating techniques. It is gold-coated across its entire surface with multiple slits of 10–20 μm in width. Its two-dimensional shape is deformed into a three-dimensional shape when used for fluid separation due to hydrodynamic forces. By adjusting the pressure applied to the microfilter, the size of the gap created by deformation can be changed. To effectively isolate the target substance, the relationship between the solution flow rate and the extent of microfilter deformation was investigated. The filtration experiments demonstrated the microfilter's ability to isolate the target substance with elastic deformation without undergoing plastic deformation. Additionally, modification of the microfilter surface with nucleic acid aptamers resulted in the selective isolation of the target cell, which further demonstrates the potential application of microfilters in the isolation of specific components of heterogeneous solutions.

Published under license by AIP Publishing. <https://doi.org/10.1063/5.0025927>

I. INTRODUCTION

We are surrounded and composed of heterogeneous solutions. For example, there are various cells in the living body, suspended particulate matter (SPM) in the atmosphere such as pollen, yellow dust, and PM2.5, as well as bacteria and viruses. Detection, isolation, and acquisition of these particles can be utilized for various purposes such as medical diagnosis, elucidation of pathological mechanisms, and treatment. Furthermore, environmental studies such as evaluating substances in the air and water and assessing their impact on living organisms can be performed (Lee *et al.*, 2020; Kanaoka, 2019). Existing methods of capturing a target substance use fiber and

porous filters that take advantage of the difference in filter pore size and target substance size. In conventional filters, substances larger than the filter pore size are collected, making it difficult to selectively capture target substances (Zhou *et al.*, 2019; Sollier *et al.*, 2014; Umezawa and Nuri, 1989; and Kunugi, 1990). Additionally, they capture non-target substances that are larger than or equal to the size of the target substances, and hence, it is difficult to separate the target substances from a variety of captured particles. Furthermore, methods that use dielectrophoretic force (Fabbri *et al.*, 2013; Gascoyne and Shim, 2014; Jen, Chang, Huang, and Chen, 2012; and Chan *et al.*, 2018) to separate molecules introduce the suspension

containing the target substance into an inhomogeneous electric field to generate a difference in the dielectric constant between the target substance and the solution. This difference creates an electric field gradient that, in turn, gives rise to the dielectrophoretic force, allowing separation of the target substance. However, the problem with these methods is that the separation performance is low in a highly concentrated suspension, hindering continuous processing.

Meanwhile, methods based on antigen–antibody reactions such as ELISA (Enzyme-Linked Immunosorbent Assay) and immunosorbing techniques are being widely used (Rieddorf *et al.*, 2007; Wasniewski *et al.*, 2013; Hammami *et al.*, 2017; and Revzin, Maverakis, and Chang, 2012). These methods draw on the specific binding between antigen and antibody and can specifically detect the target substance if no cross-reaction occurs. The capture of a target substance using an antibody has been performed (Nagrath *et al.*, 2007; Liu *et al.*, 2020; Wu *et al.*, 2019). In this study, we fabricated microfilters with the capacity to isolate target substances that cannot be otherwise isolated only by size via combining size-selective and affinity-selective isolation methods. Hence, this study aimed to develop a microfilter that can selectively isolate the target particle.

II. MATERIALS AND METHODS

A. Overview of the dynamically deformable microfilter and measurement of microfilter deformation

Figure 1 shows the schematic diagram of the microfilters. Unlike conventional filters that separate substances by pore size,

these microfilters have slits. This structure allows them to be deformed from a two-dimensional to a three-dimensional form due to hydrodynamic forces. The microfilter in Fig. 1(a) has a comb-shaped structure in which deformation starts at the root by applying hydrodynamic forces, causing platelike elements to intersect with each other. The microfilter in Fig. 1(b) is a structure with multiple slits arranged in arcs, which are bent by hydrodynamic forces to form a shape resembling an insect net. These microfilters were fabricated using photolithography and electroplating techniques. Furthermore, the entire surface was gold-plated to enable modifications of molecules such as antibodies and DNA aptamers for the selective capture of the target substance. In this study, the microfilters were designed for target substances that were about the size of a cell ($20\text{ }\mu\text{m}$). Specifically, two slit widths (S) of $10\text{ }\mu\text{m}$ and $20\text{ }\mu\text{m}$ were used. The microfilter deformation was measured using a microscope USB (Universal Serial Bus) camera with a zoom lens (YCU-300 F, Yashima Optical Co., Ltd.) by comparing the filter shapes before and after deformation.

B. Isolating the target substance using the microfilter

The microfilters separate the target substance using both size separation, which results from microfilter deformation, and affinity separation by antibodies or aptamers, which modify the microfilter surface. Figure 2(b) describes the separation procedure of molecules using the microfilter. The principle of separation is as follows: the microfilter has slits finer than the target substance diameter. When a solution containing the target substance is poured into the

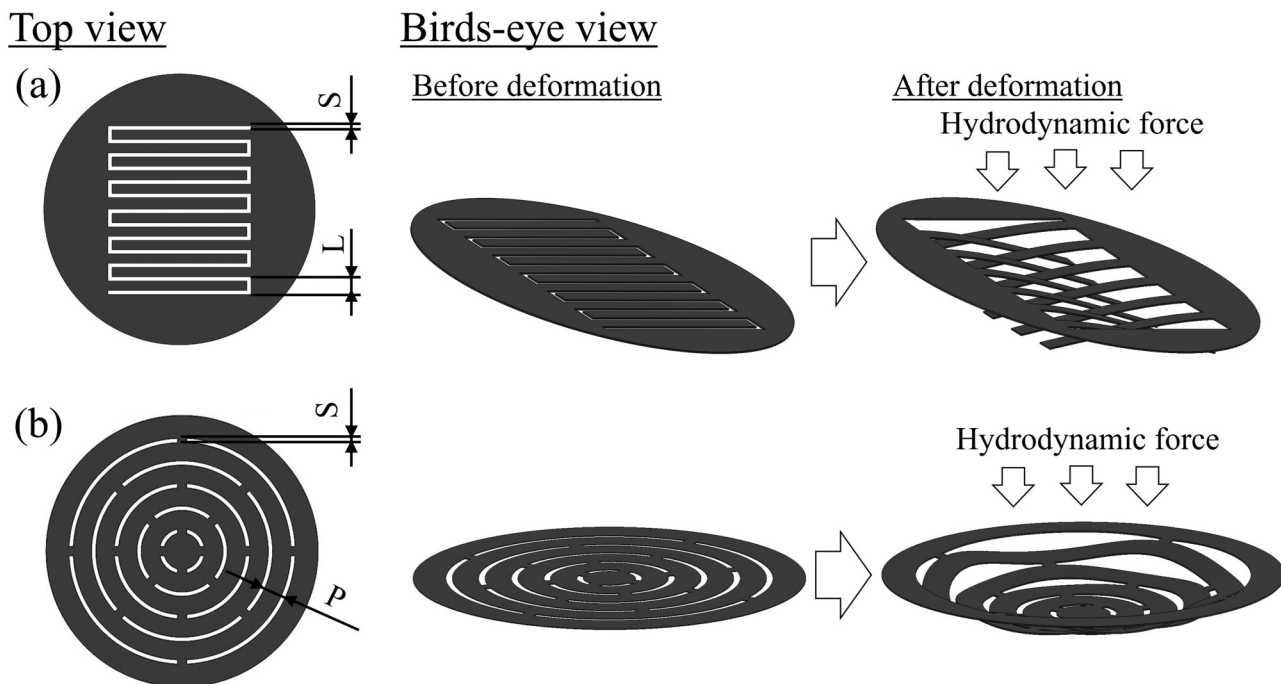


FIG. 1. Overview of dynamically deformable microfilters. (a) Schematic of a microfilter with a comb-shaped structure. (b) Schematic of a microfilter with an arc-shaped multiple slit structure. The two microfilters with a 15 mm diameter were designed having $10\text{ }\mu\text{m}$ and $20\text{ }\mu\text{m}$ slit widths (S). The slit length (L) was $500\text{ }\mu\text{m}$ and the slit interval (P) $250\text{ }\mu\text{m}$.

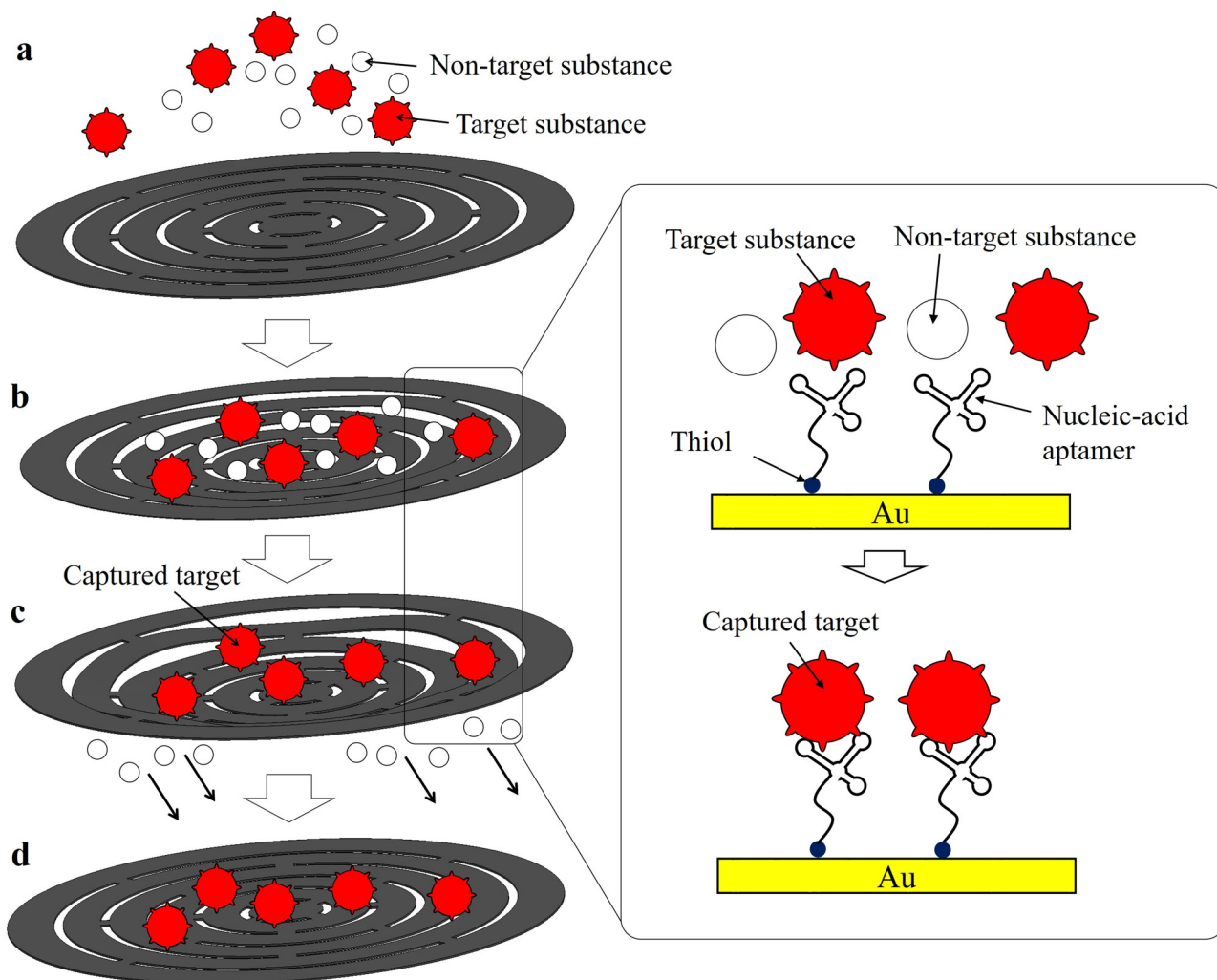


FIG. 2. Target substance separation procedure using the microfilter. (a) Initial state of the microfilter. (b) Clogging of all substances to the microfilter. (c) The microfilter deformation and releasing of the non-target substance. (d) Selective isolation of the target substance.

microfilter at a constant rate, hydrodynamic forces influence the microfilter, causing it to be elastically deformed into a certain shape [Fig. 2(a)].

The degree of elastic deformation can be adjusted according to the flow rate. Substances larger in size than the slit, including the target substance, are trapped by the microfilter, causing clogging of the slit [Fig. 2(b)]. If solution feeding continues, clogging increases, and simultaneously the hydrodynamic forces applied on the microfilter become progressively larger, causing the microfilter to deform further and the slit opening to become wider. In this process, the target substance remains on the microfilter surface by specific interaction with the antibodies or aptamers modified on the microfilter, while the non-target substances flow out from the slits [Fig. 2(c)]. Once the non-target cells flow out of the slits, the hydrodynamic forces applied on the microfilter become small,

causing the microfilter to return to its original shape. In this way, the target substance is isolated and acquired [Fig. 2(d)]. In this respect, the presented microfilter is more advantageous than general filters (Huang *et al.*, 2014) and filters described in other studies (Sarioglu *et al.*, 2015).

C. Fabrication of the microfilter

The fabrication process of the dynamically deformable microfilter is shown in Fig. 3. The microfilter is a metallic structure developed using photolithography and electroplating techniques. In the photolithographic process, a spin coater (MS-A150, Mikasa Corporation) was used to apply a 30 μm -thick positive photoresist (AZ P4903, Merck Performance Materials Ltd.) on the copper substrate [Fig. 3(a)], which was subsequently exposed by UV light

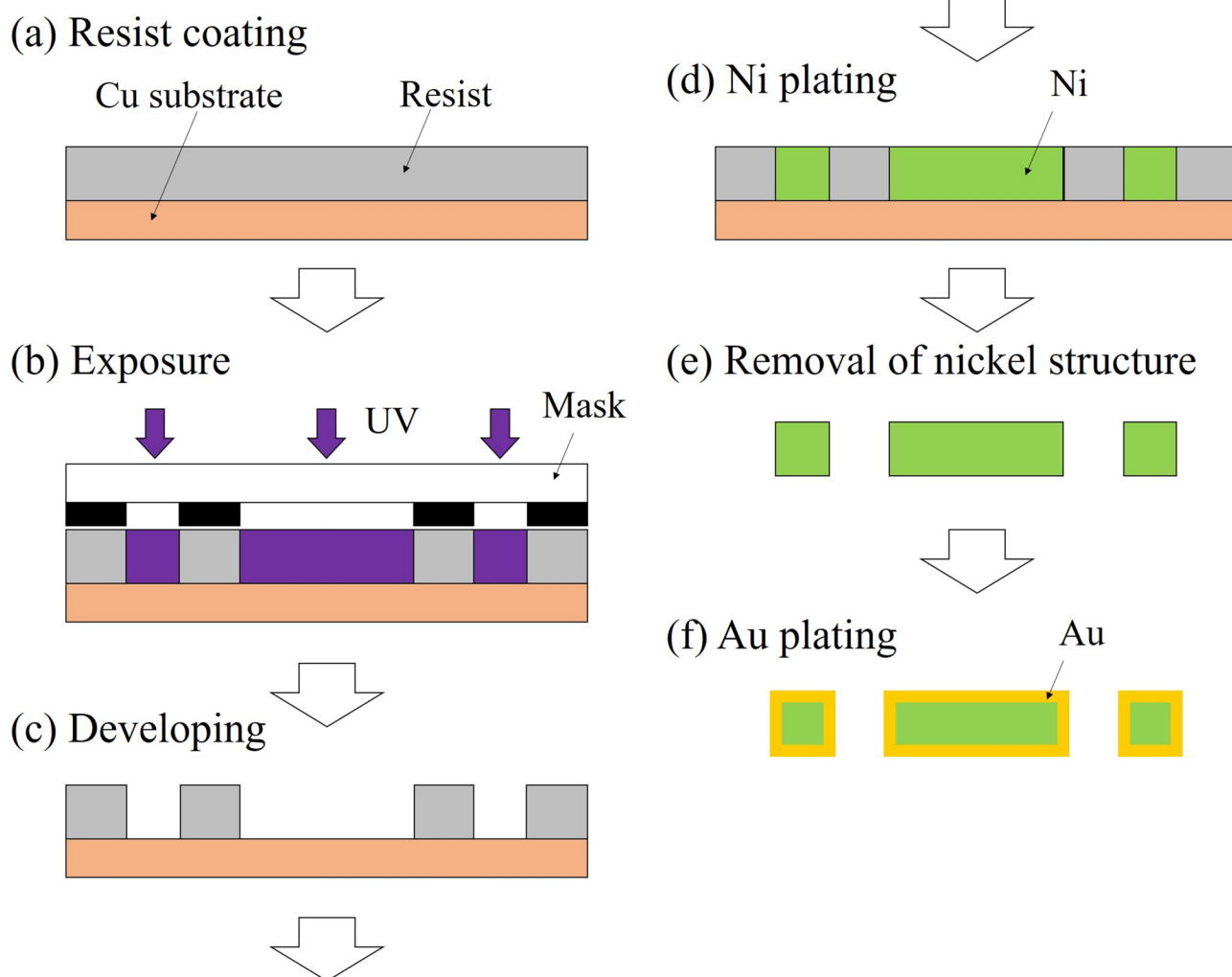


FIG. 3. Procedure of microfilter fabrication. (a) Photoresist coating on the Cu substrate. (b) Photoresist curing by UV exposure. (c) Microfilter mold creation by photoresist development. (d) Fabrication of the microfilter structure on the Cu substrate by nickel electroplating. (e) and (f) Removal of the nickel structure and Au electroplating to cover the structure surface.

(1.75 J/cm^2) using a mask aligner (MA-20, Mikasa Corporation) [Fig. 3(b)]. The photoresist was developed using the AZ 400K Developer (Merck Performance Materials, Ltd.) to form a resistant structure, which would serve as a mold [Fig. 3(c)]. Subsequently, the nickel structure was fabricated by an electroplating process [Fig. 3(d)]. The nickel structure was released from the copper substrate [Fig. 3(e)]. Finally, the entire surface was electroplated with gold [Fig. 3(f)].

III. RESULTS AND DISCUSSION

A. Device fabrication

Figure 4 shows images of the microfilters. Two filters (c) having different sizes of micropores ($S = 10 \mu\text{m}$, $P = 30 \mu\text{m}$;

$S = 20 \mu\text{m}$, $P = 60 \mu\text{m}$) were fabricated as controls. The microfilters were designed with a diameter and thickness of 15 mm and $25 \mu\text{m}$, respectively. The slit widths of (a) and (b) were set to $10 \mu\text{m}$ and $20 \mu\text{m}$, respectively. The microfilters were metallic structures with a high aspect ratio (microfilter thickness/slit width = 2.5). These microfilters did not have any slit defects or surface irregularities and were fabricated with great precision. In the case of microfilters with a $20 \mu\text{m}$ slit width (designed width), the fabricated width was $18.3 \mu\text{m}$ (mean value for $n = 12$), and its error was only 6%. A smaller slit width is a desirable feature for separating fine target substances. The yield of the microfilters was 90%. Since the slit widths of dynamically deformable microfilters can be controlled by adjusting the flow rates of liquids passing through these

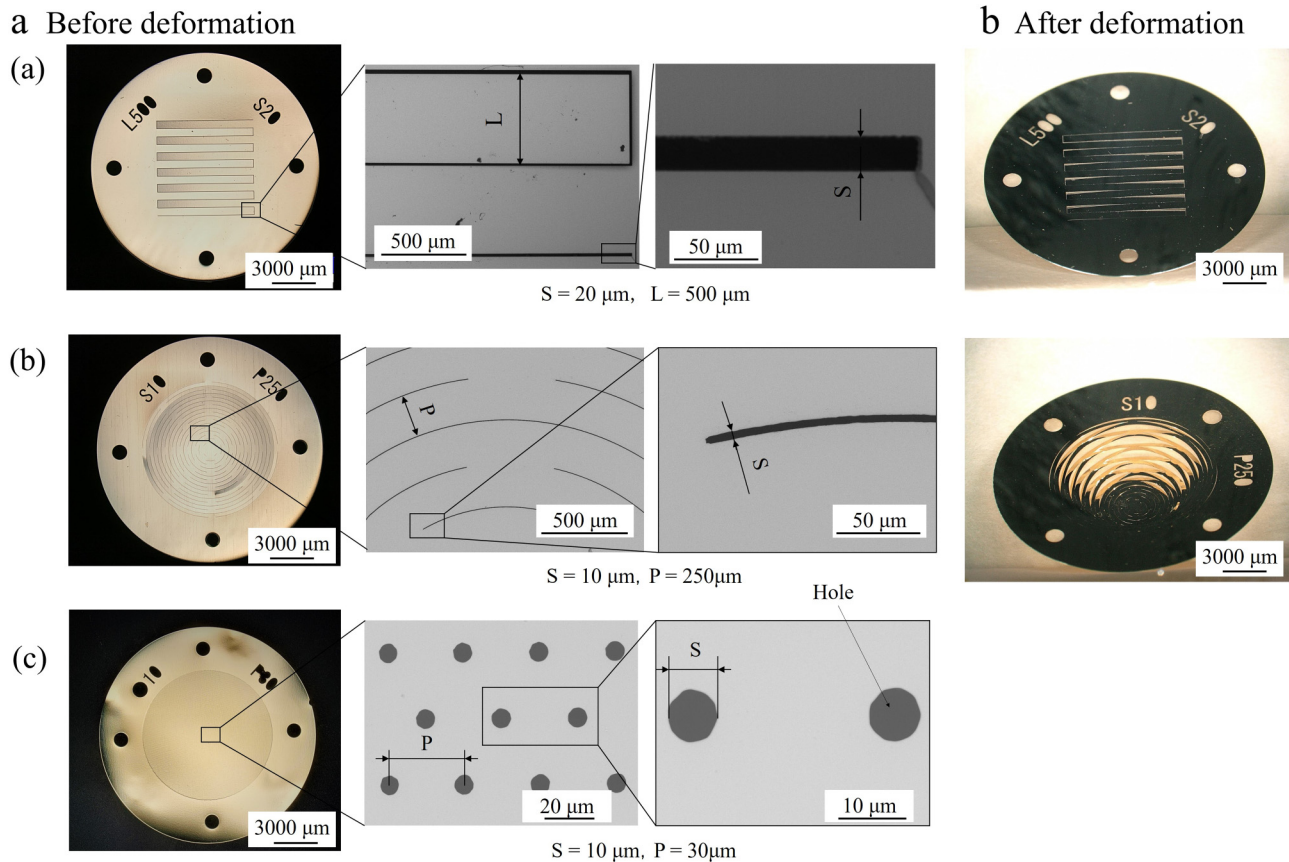


FIG. 4. Images of the fabricated microfilters. (a) Photographs of the fabricated microfilter with a comb-shaped structure. (b) Photographs of the fabricated microfilter with an arc-shaped multiple slit structure. (c) Photographs of the fabricated 2D filter having a micro-hole array. 3D microfilters have great precision and an elastic structure, which help them return to their original shape when deformed by hydrodynamic forces. A 2D filter is a filter manufactured with the same process and materials used for 3D filters. The 2D filter has holes of 10 μm or 20 μm in diameter arranged in an array and does not deform into a three-dimensional shape.

microfilters, they are expected to be applied on target substances of various sizes.

B. Measurement of filter deformation

The basic properties of the microfilters were evaluated. The microfilter was fixed to the filter holder, as shown in Fig. 5(a), and inserted into the housing. The experimental setup is shown in Fig. 5(b) and was used to measure the extent of filter deformation. It was connected with a peristaltic tube pump, and the degree of deformation was measured at seven different flow rates (5, 10, 15, 20, 25, 30, and 40 ml/min).

The relationship between the flow rate and the degree of microfilter deformation is shown in Fig. 6. In microfilter (a), the deformation was approximately 110, 350, and 820 μm at flow rates of 5, 20, and 40 ml/min, respectively. In microfilter (b), the deformation was approximately 40, 60, and 90 μm at 5, 20, and 40 ml/min, respectively. The deformation of both microfilters increased linearly with the increase in the flow rate. The deformed microfilters returned to their original state when the liquid flow was stopped, suggesting

that the deformation was within the elastic range under the flow rate conditions set for this experiment (5–40 ml/min). A comparison between microfilter (a) and (b) revealed that the deformation was smaller in microfilter (b), suggesting that it was more appropriate for the filtration of fine particles. Microfilter (a) had a relatively simple comb structure, and the deformation started from the base of the comb structure. Therefore, the deformation can be calculated from the triangle similarity. For example, at a flow rate of 5 ml/min, if the total slit length was about 6 mm, the overall deformation was approximately 100 μm . This indicates that the slit gap was more than 20 μm at a 1.2 mm point from the deformed base.

For microfilters (a) and (b), finite element analysis (ANSYS 19.2, ANSYS Inc.) was used to analyze the microfilter deformation (Fig. 7). Conditions used in this analysis are shown in Table I. The deformation of the entire microfilter (a) at a 5 ml/min flow rate was approximately 120 μm . Almost no deformation was observed at the center of microfilter (b), though the outer slit of this microfilter was greatly deformed. The deformation of the entire microfilter (b) at the flow rate of 5 ml/min was approximately 40 μm , and the slit

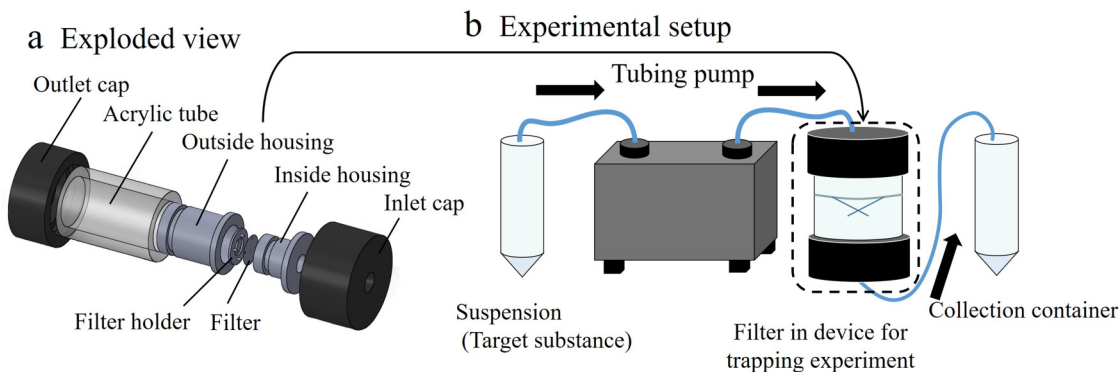


FIG. 5. Overview of the experimental design to separate the target substance. The microfilter is installed in the device housing (a), and a suspension containing the target substance is transferred to the device using a tube pump (b).

gap was at most $20\text{ }\mu\text{m}$. These results suggest that the fluid passed at a flow rate lesser than 5 ml/min separates the target cell most efficiently. In addition, the measured deformation and simulation results were compared to each other; under the condition of a flow rate of 5 ml/min , microfilter (a) showed a deformation (simulation value) of about $120\text{ }\mu\text{m}$, and the measurement result was $110\text{ }\mu\text{m}$, whereas microfilter (b) showed a deformation (simulation value) of about $40\text{ }\mu\text{m}$, and the measurement result was $40\text{ }\mu\text{m}$. Thus, these values showed good agreement. Furthermore, as for microfilters (a) and (b), structural and fluid coupled analysis was performed to analyze the shear stress; no clear correlation was found between the deformation of the microfilter and shear stress (Fig. 2 in the supplementary material).

C. Filtration efficiency of PMMA particles

Filtration experiments were conducted using monodisperse poly (methyl methacrylate) spherical particles (PMMA, Soken

Chemical Co., Ltd.) with a mean particle size of $19.3\text{ }\mu\text{m}$, which was about the same size as the target substance. The PMMA particles were mixed with ultrapure water and passed through the microfilter. The particles in the flow-through were counted using the hemocytometer, and the filtration efficiency was obtained using formula (1),

$$(n_{in} - n_{out})/n_{in} \times 100. \quad (1)$$

Here, n_{in} and n_{out} denote the number of PMMA particles before and after the solution was passed through the microfilter, respectively. The concentration of the PMMA particles was adjusted to 1.0×10^6 particles/ml before the solution was passed through the filter. As a control, the same experiments were performed using filter (c). Three different flow rates, 1, 5, and 10 ml/min , were used. The experiments were performed in triplicate. The filtration

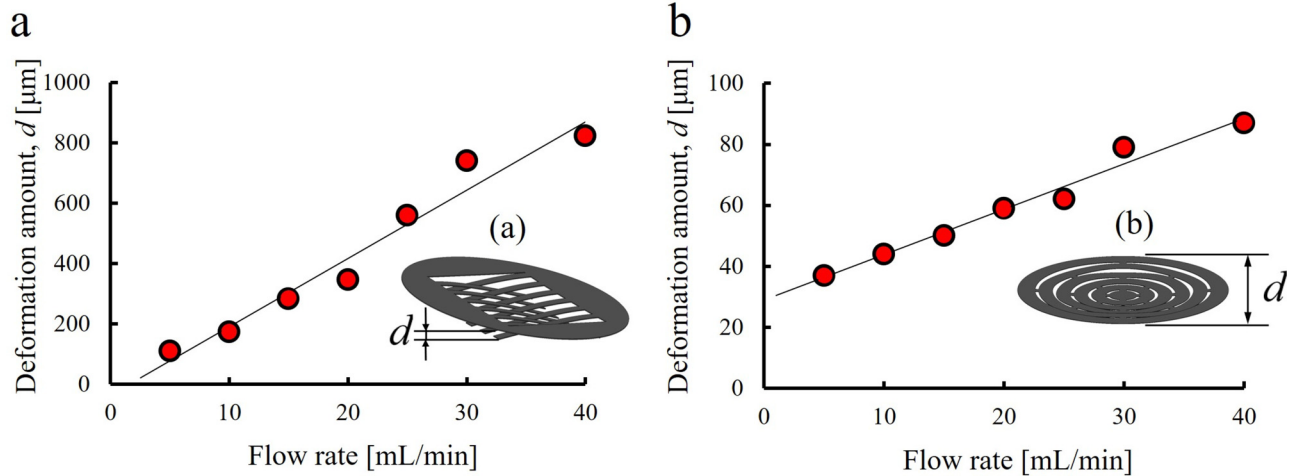


FIG. 6. Evaluation of deformation of microfilters [(a) and (b)]. The deformation of the microfilter increases linearly with an increasing flow rate.

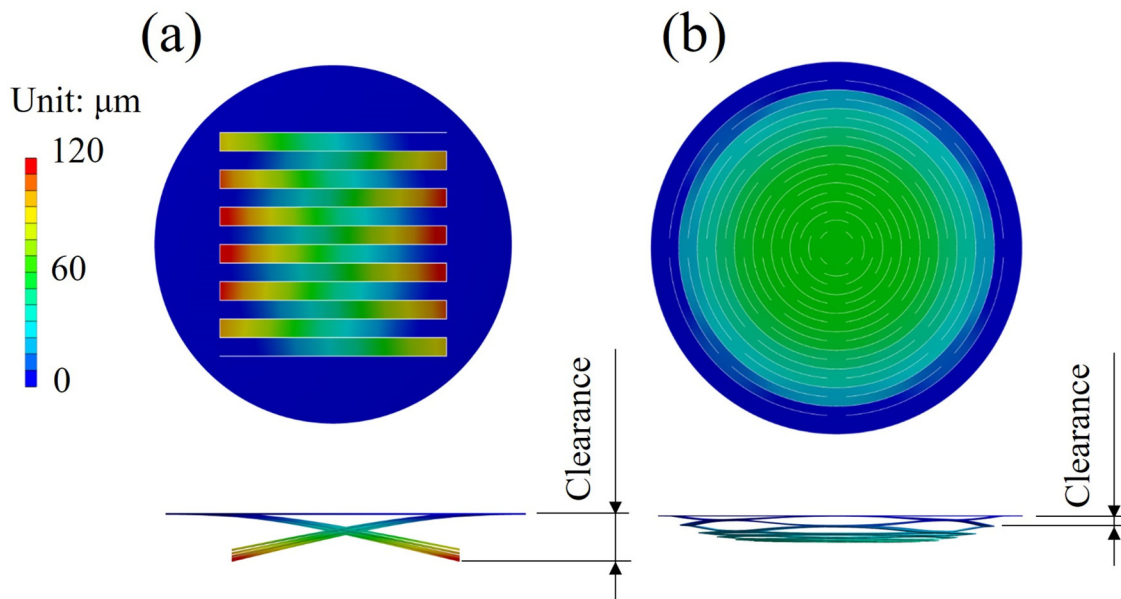


FIG. 7. Analysis of the deformation of microfilters [(a) and (b)] by the finite element method using ANSYS. The amount of displacement from the reference plane when the hydrodynamic force applied to the microfilter from top to bottom is shown. Microfilter (a) deformed from the base of the comb structure, and the amount of displacement was $120\text{ }\mu\text{m}$ at most. In addition, the slit gap deformation of microfilter (b) showed almost no deformation in the range of $\varphi 6\text{ mm}$ from the center and was about $10\text{ }\mu\text{m}$ at $\varphi 8\text{ mm}$ and at most $20\text{ }\mu\text{m}$ at $\varphi 10\text{ mm}$. Therefore, almost no deformation was noted at the microfilter center, and the slit gap deformation became greater toward the outer edge.

efficiency for the PMMA particles in microfilters (a)–(c) by flow rate is shown in Fig. 8.

In all filters, the filtration efficiency for the PMMA particles increased with a decreasing flow rate. In 3D filters (a) and (b), the filtration efficiency was thought to decrease as the slit gap widened with an increasing flow rate, allowing the PMMA particles to pass through the filter without being trapped. Furthermore, with respect to the slit width of microfilters (a) and (b), the efficiency for a slit width of $20\text{ }\mu\text{m}$ was higher than that for a slit width of $10\text{ }\mu\text{m}$. The maximum filtration efficiency was about 80% at a flow rate of 1 ml/min . A possible reason for the low efficiency of the microfilter with a slit width of $10\text{ }\mu\text{m}$ is that the trapped PMMA particles clog the slit, causing the flow channels to become narrow and accelerate the fluid passing through the microfilter. Herewith, it is conceivable that the trapped particles were washed away, or the amount of

deformation of the microfilter was increased and may not be trapped. Furthermore, with the slit width of $20\text{ }\mu\text{m}$ and a flow rate of 5 ml/min , microfilter (b) showed a filtration efficiency of about 40%, approximately twice that of (a). Microfilter (b) had a smaller degree of deformation than that of microfilter (a), and hence, was able to capture more PMMA particles. Figure 9 shows an SEM image of the three-dimensional filters (a) and (b) obtained after the PMMA particle filtration. It was confirmed that the dynamically deformable microfilters could capture the target substances with their filter structures. It is important to note that the PMMA particles trapped in the microfilters had fallen away from the slit space of the microfilters during our observations. Moreover, the filtration efficiency of the 2D filters was around 60% at the minimum flow rate of 1 ml/min , indicating that the 3D filters were more effective in trapping substances with the size of a cell.

D. Target cell separation using the microfilter

The target particle size is $20\text{ }\mu\text{m}$, which is similar to the size of a living cell. Separation based solely on size has the following problems: target substances may pass through the filter; non-target substances of the same or greater sizes may simultaneously be captured. Cancer cells were selected to demonstrate the feasibility of separating small target cells from a solution containing an enormous number of foreign substances. Cancer cells are known to circulate in small numbers in the blood of patients (Plaks, Koopman, and Werb, 2013; Cristofanilli *et al.*, 2004; Scher *et al.*, 2015; Hou *et al.*, 2012; Bouab *et al.*, 2019; Muhanna *et al.*, 2015; Iliescu

TABLE I. Conditions for microfilter deformation analysis.

Item	Boundary condition
Analysis model	Axis-symmetric
Young's modulus	200 GPa
Number of nodes	1 049 655
Number of elements	414 361
Element type	PLANE182 (2D four-node structural solid)

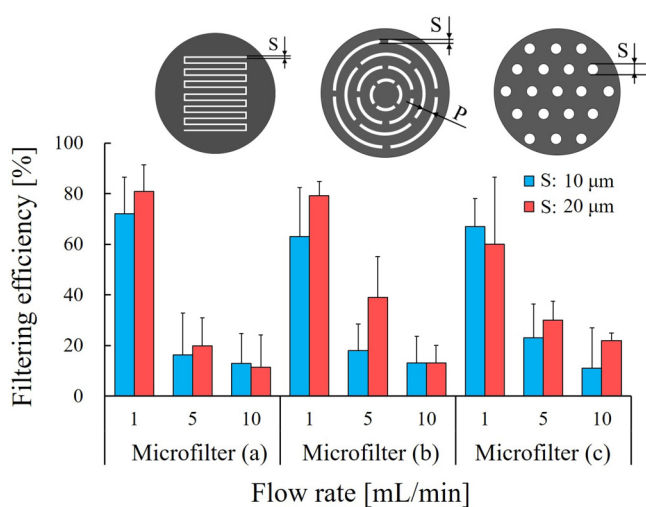


FIG. 8. Evaluation of the filtration efficiency of PMMA particles.

et al., 2019). Our study's technique can be applied to cancer diagnosis if the cancer cells can be specifically separated from the blood. Since it is known that epithelial cell adhesion molecule (EpCAM) is highly expressed on the surface of many cancer cells ([Baeuerle and Gires, 2007](#); [Went *et al.*, 2004](#); [Patriarca *et al.*, 2012](#)), microfilter (b) was modified with an EpCAM aptamer (5'-TTT

TTT TCA CTA CAG AGG TTG CGT CTG TCC CAC GTT GTC ATG GGG GGT TGG CCT G-3') that was capable of specifically binding to EpCAM. The point by point binding between the aptamer and EpCAM is not strong. However, EpCAM is abundantly expressed on the cancer cell membrane, and aptamers bind to it; thus, it has the same binding power as that of antibodies. Since multiple aptamers modified on the substrate and multiple EpCAMs on the cell membrane bind to each other, it has been shown that the binding force is strong when viewed in terms of the whole cell ([Song *et al.*, 2013](#)). Subsequently, a self-assembled monolayer (SAM layer) was formed by adding 10 μM 6-hydroxy-1-hexanethiol solution to the microfilter to minimize non-specific absorption. This allowed the non-target cells, such as blood cells, to pass through the microfilter without being adsorbed onto the microfilter surface, whereas only target cells were specifically trapped and collected on the microfilter surface.

As a control, scrambled DNA (5'-TTT TTT TTT TCG TGG TGA GAA GTC GAG TGG TGC TGC TCC AGT TGC TGT CCA TCG TCC G-3'), consisting of the same nucleobase sequence as that of the EpCAM aptamer, was evaluated. MDA-MB-453 (human breast-cancer-derived cell) and HEK293 T (human embryonic kidney 293 T cells) were used as the controls for target and non-target cells, respectively. The cells were prepared at a 5.0×10^4 cells/ml concentration and poured into the microfilter at a flow rate of 0.5 ml/min. Subsequently, the number of captured cells per unit area was evaluated by staining cell nuclei and observing them by fluorescence microscopy.

The fluorescence images of cells captured by the microfilter are shown in [Fig. 10](#). When the microfilter surface was

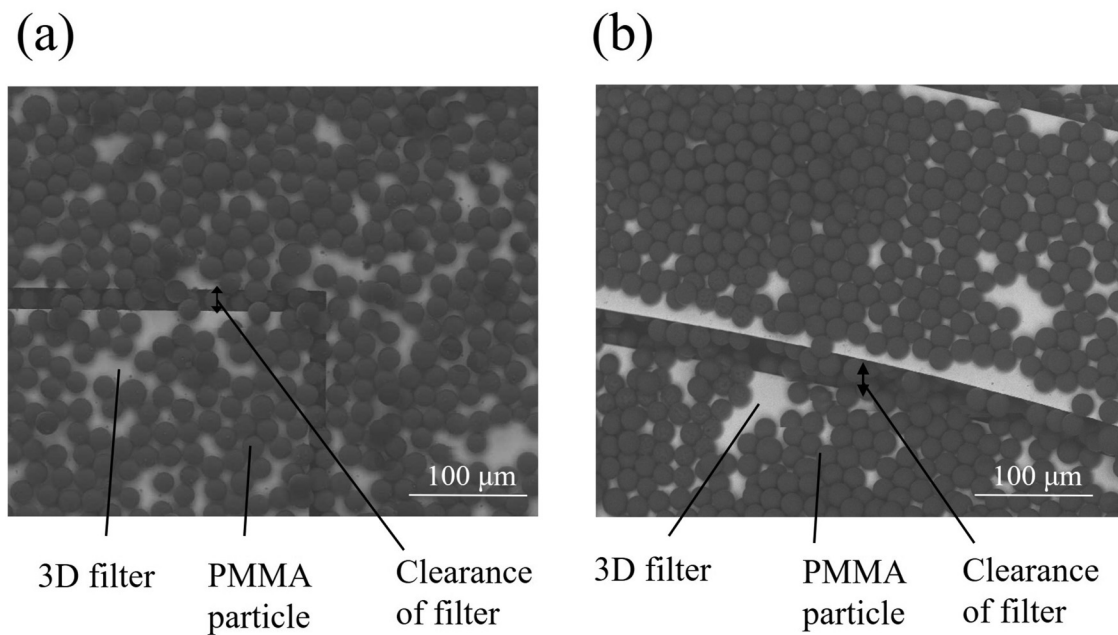
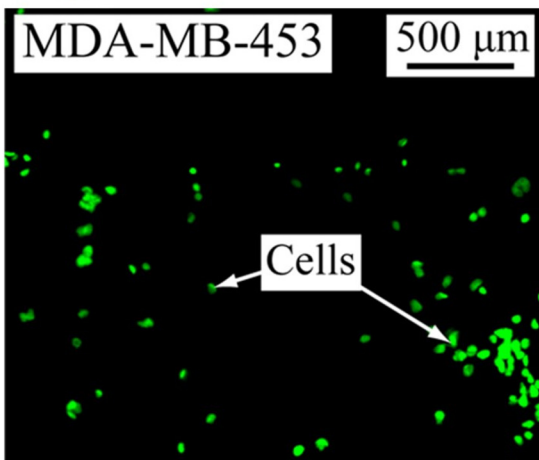


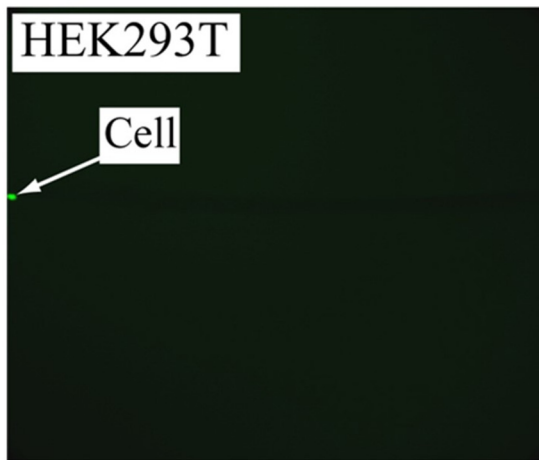
FIG. 9. Image of PMMA particles captured by microfilters. (a) Result of using the comb structure microfilter. (b) Result of using the arc-shaped multiple slit structure.

◆ Aptamer

a

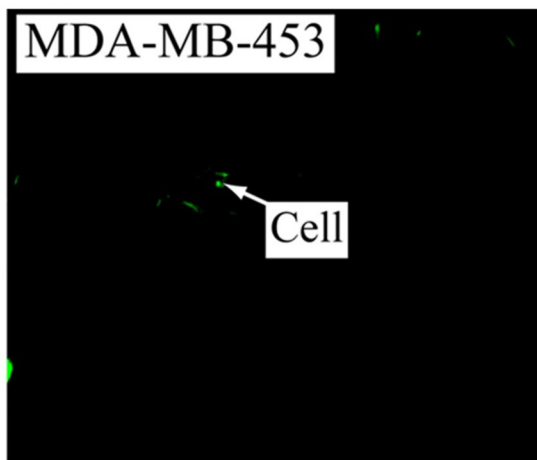


b



◆ Scrambled DNA

c



d

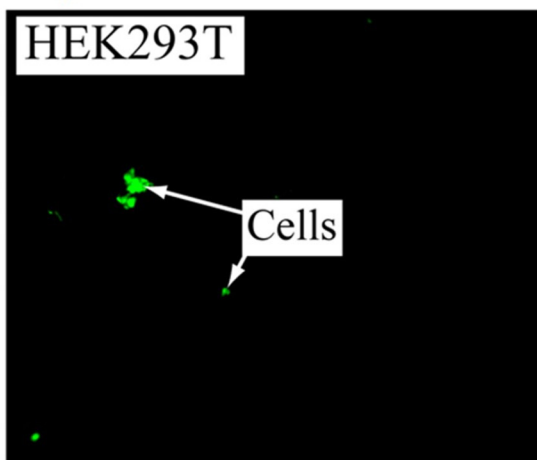


FIG. 10. Fluorescence images of cancer cells (MDA-MB-453) and normal cells (HEK 293 T) on the microfilter modified with the aptamer or scrambled DNA. In the case of using the microfilter modified with the EpCAM aptamer, (a) cancer cells were specifically captured, and (b) non-specific adsorption of normal cells was inhibited. In the case of using the microfilter modified with scrambled DNA, (c) cancer cells were not specifically captured, and (d) non-specific adsorption of normal cells was almost inhibited.

modified with the EpCAM aptamer, cancer cells were specifically captured [Fig. 10(a)], while non-specific absorption of normal cells was inhibited [Fig. 10(b)]. When the microfilter surface was modified with the scrambled DNA, only a small number of cancer cells and normal cells were absorbed by the microfilter, and non-specific absorption was inhibited [Figs. 10(c) and 10(d)]. In contrast, in a preliminary experiment in which the aptamer was not modified with a microfilter, almost no cancer cells could be captured.

Figure 11 shows the number of cells captured per unit area by the microfilter. The number of captured cancer cells and normal cells were 64 and 1.7, respectively, and the number of cancer cells captured by the specific capture effect of the EpCAM aptamer was about 40 times that of the normal cells. In contrast, when the microfilter surface was modified with the scrambled DNA, the number of cancer cells and normal cells captured were 0.7 and 10, respectively, showing that the non-specific absorption was inhibited.

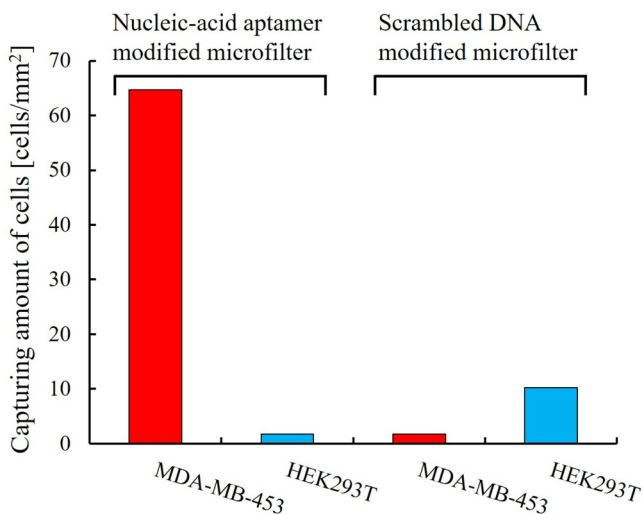


FIG. 11. Cancer and normal cells captured by the aptamer-modified microfilter.

The objective is to separate the target substance from a large amount of foreign substances. To prove that this objective can be achieved, we carried out the cancer cell isolation experiments by mixing normal cells and cancer cells. The total number of cells was 5.0×10^4 cells. The ratios of normal and cancer cells were 9:1, 1:1, and 1:9. The number of captured cells per unit area are summarized and compared between 2D filter (c) and 3D microfilter (b) modified with the EpCAM aptamer in Fig. 12. In the case of the microfilter with a slit width of 10 μm , the number of cancer and normal cells captured were 4.1 and 1.4, respectively, when the cancer to normal cell ratio was 1:1. These results indicate that

approximately three times more cancer cells were captured as compared to normal cells. Similarly, at a 1:9 ratio of cancer to normal cells, the number of cancer and normal cells captured were 2.1 and 4.7, respectively. These results demonstrate that the filter could inhibit non-specific absorption and selectively separate cancer cells in a solution where the number of normal cells was nine times greater than that of cancer cells. Compared with the microfilter with a slit width of 20 μm , a slit width of 10 μm was able to capture more cancer cells. This result implies that as the microfilter slit width became narrower, the cancer cells were size-selectively trapped onto the microfilter surface, allowing an affinity-selective specific capture of cells. Besides, since the main component of cells is water, hydrodynamic forces deform the shape of cells on the filter, effectively increasing the contact area and yielding a more efficient capture of cells. These results indicate that the cancer cells were continuously captured without being released from the microfilter by the specific binding effect of the EpCAM aptamer on the microfilter surface, even when the cancer cells clogged the microfilter and the hydrodynamic force applied to the microfilter increased. In addition to the function to selectively capture the size of 20 μm or more, similar to conventional filters, experiments showed the microfilter applicability in the capture and separation of various substances. In this way, the optimization of the flow rate for specific binding of the EpCAM aptamer, the target substance, and changing the microfilter shape resulted in the specific separation of the target cells.

IV. CONCLUSIONS

Dynamically deformable microfilters were fabricated to selectively isolate the target substance from a solution. The flow rate, the degree of deformation, and the filtration efficiency were evaluated as basic properties of the microfilters. It was demonstrated that no plastic deformation of the microfilters occurred at the set

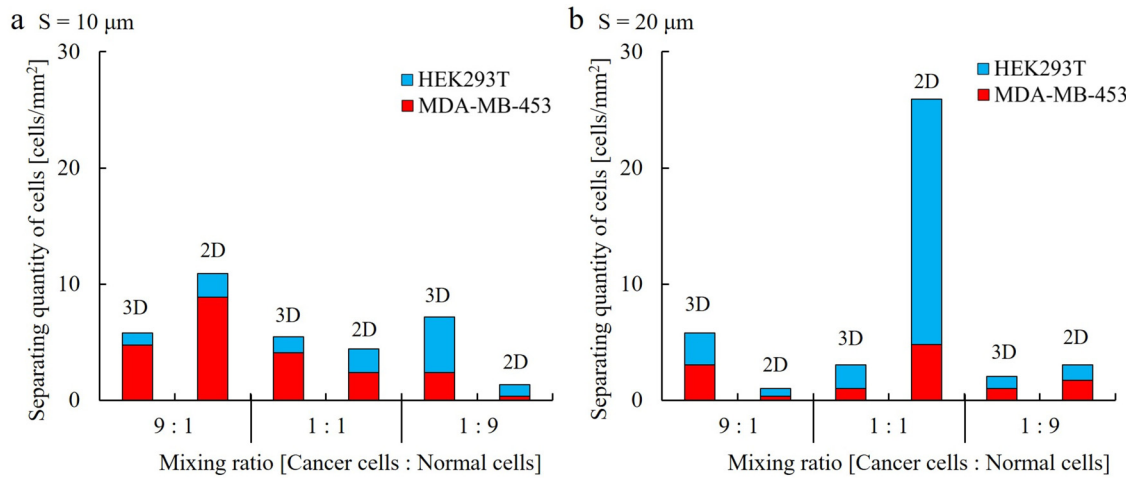


FIG. 12. Comparison of cancer and normal cell separation using different three-dimensionally deformable microfilters. (a) Result of using the microfilter with a 10 μm slit width. (b) Result of using the microfilter with a 20 μm slit width.

flow rate range of 5 to 40 ml/min, and the deformation occurred within the elastic range. The two microfilters were deformed linearly in accordance with the flow rate. The filtration efficiency at a flow rate of 1 ml/min was approximately 80% for both filters (a) and (b), and they successfully isolated the target substance in a size-selective manner. The filtration efficiency of filter (c) with pores was approximately 60% under the same condition. Furthermore, modification of the microfilter surface with nucleic acid aptamers, which specifically bind to cancer cells, demonstrated that cancer cells could be selectively separated from a pool of heterogeneous cell types.

SUPPLEMENTARY MATERIAL

See the [supplementary material](#) (Figs. 1 and 2) for a fluorescence image of cancer cells (MDA-MB-453) on the microfilter modified without the aptamer, and simulation analysis results of shear stress for microfilters (a) and (b), respectively. Please refer to Table 1 in the [supplementary material](#) for the conditions set during the microfilter shear stress analysis.

ACKNOWLEDGMENTS

This work was partly supported by a fund from the Japan Society for the Promotion of Science (JSPS) KAKENHI, via the Grant-in-Aid for Young Scientists (A) 16H06078, the Ministry of Economy, Trade and Industry (METI) under projects to support the advancement of strategic core technologies (No. 17939048). The funding sources were not involved in study design, concept, data collection, analysis, interpretation, manuscript preparation, and submission. The authors declare that they have no conflicts of interest. We would like to thank Editage (www.editage.com) for English language editing.

DATA AVAILABILITY

The data that support the findings of this study are available from the corresponding author upon reasonable request.

REFERENCES

- Baeuerle, P. A. and Gires, O., "EpCAM (CD326) finding its role in cancer," *Br. J. Cancer* **96**, 417–423 (2007).
- Bouab, E., Jiménez-Zenteno, A. K., Estève, A., Bourrier, D., Vieu, C., and Cerf, A., "Fabrication of 3D microdevices from planar electroplating for the isolation of cancer associated cells in blood," *Microelectron. Eng.* **213**, 69–73 (2019).
- Chan, J., Kayani, A., Ali, M., Kok, C., Majlis, B., Hoe, S., Marzuki, M., Khoo, A., Ostrikov, K., Rahman, M., and Sriram, S., "Dielectrophoresis-based microfluidic platforms for cancer diagnostics," *Biomicrofluidics* **12**, 011503 (2018).
- Cristofanilli, M., Budd, G. T., Ellis, M. J., Stopeck, A., Matera, J., Miller, M. C., Reuben, J. M., Doyle, G. V., Allard, W. J., Terstappen, L. W. M. M., and Hayes, D. F., "Circulating tumor cells, disease progression, and survival in metastatic breast cancer," *N. Engl. J. Med.* **351**, 781–791 (2004).
- Fabbri, F., Carloni, S., Zoli, W., Ulivi, P., Gallerani, G., Fici, G., Chiadini, E., Passardi, A., Frassineti, G., Ragazzini, A., and Amadori, D., "Detection and recovery of circulating colon cancer cells using a dielectrophoresis-based device: KRAS mutation status in pure CTCs," *Cancer Lett.* **335**, 225–231 (2013).
- Gascoyne, P. and Shim, S., "Isolation of circulating tumor cells by dielectrophoresis," *Cancers* **6**, 545–579 (2014).
- Hammami, M. B., Chhaparia, A., Piao, J., Zhou, Y., Hachem, C., and Lai, J., "Mixed adenocarcinoma and squamous cell carcinoma of duodenum: A case report and review of the literature," *Case Rep. Gastroenterol.* **11**, 402–410 (2017).
- Hou, J. M., Krebs, M. G., Lancashire, L., Sloane, R., Backen, A., Swain, R. K., Priest, L. J. C., Greystoke, A., Zhou, C., Morris, K., Ward, T., Blackhall, F. H., and Dive, C., "Clinical significance and molecular characteristics of circulating tumor cells and circulating tumor microemboli in patients with small-cell lung cancer," *J. Clin. Oncol.* **30**, 525–532 (2012).
- Huang, T., Jia, C., Jun-Yang, S. W., Zhang, H. W., Cong, H., Jing, F., Mao, H.-J., Jin, Q.-H., Zhang, Z., Chen, Y., Li, G., Mao, G., and Zhao, J., "Highly sensitive enumeration of circulating tumor cells in lung cancer patients using a size-based filtration microfluidic chip," *Biosens. Bioelectron.* **51**, 213–218 (2014).
- Iliescu, F., Poenar, D., Yu, F., Ni, M., Chan, K., Cima, I., Taylor, H., Cima, I., and Iliescu, C., "Recent advances in microfluidic methods in cancer liquid biopsy," *Biomicrofluidics* **13**, 041503 (2019).
- Jen, C., Chang, H., Huang, C., and Chen, K., "A microfabricated module for isolating cervical carcinoma cells from peripheral blood utilizing dielectrophoresis in stepping electric fields," *Microsyst. Technol.* **18**, 1887–1896 (2012).
- Kanaoka, C., "Fine particle filtration technology using fiber as dust collection medium," *KONA Powder Part. J.* **36**, 88–113 (2019).
- Kunugi, M., "A review of current methods for the determination of particulate," *J. Jpn. Soc. Air Pollution* **25**, 355–370 (1990).
- Lee, M., Choi, H., Kumita, M., and Otani, Y., "Present status of air filters and exploration of their new applications," *KONA Powder Part. J.* **37**, 19–27 (2020).
- Liu, H.-Y., Koch, C., Haller, A., Joosse, S. A., Kumar, R., Vellekoop, M. J., Horst, L. J., Keller, L., Babayan, A., Failla, A. V., Jensen, J., Peine, S., Keplinger, F., Fuchs, H., Pantel, K., and Hirtz, M., "Evaluation of microfluidic ceiling designs for the capture of circulating tumor cells on a microarray platform," *Adv. Biosyst.* **4**, 1900162 (2020).
- Muhanna, N., Mepham, A., Mohamadi, R. M., Chan, H., Khan, T., Akens, M., Besant, J. D., Irish, J., and Kelley, S. O., "Nanoparticle-based sorting of circulating tumor cells by epithelial antigen expression during disease progression in an animal model," *Nanomedicine* **11**, 1613–1620 (2015).
- Nagrath, S., Sequist, L. V., Maheswaran, S., Bell, D. W., Irimia, D., Ulkus, L., Smith, M. R., Kwak, E. L., Digumarthy, S., Muzikansky, A., Ryan, P., Balis, U. J., Tompkins, R. G., Haber, D. A., and Toner, M., "Isolation of rare circulating tumour cells in cancer patients by microchip technology," *Nature* **450**, 1235–1239 (2007).
- Ollier, E., Go, D. E., Che, J., Gossett, D. R., O'Byrne, S., Weaver, W. M., Kummer, N., Rettig, M., Goldman, J., Nickols, N., McCloskey, S., Kulkarni, R. P., and Carlo, D. D., "Size-selective collection of circulating tumor cells using vortex technology," *Lab Chip* **14**, 63–77 (2014).
- Patriarca, C., Macchi, R. M., Marschner, A. K., and Mellstedt, H., "Epithelial cell adhesion molecule expression (CD326) in cancer: A short review," *Cancer Treat Rev.* **38**, 68–75 (2012).
- Plaks, V., Koopman, C., and Werb, Z., "Circulating tumor cells," *Science* **341**, 1186–1188 (2013).
- Revzin, A., Maverakis, E., and Chang, H., "Biosensors for immune cell analysis—A perspective," *Biomicrofluidics* **6**, 021301 (2012).
- Riethdorf, S., Fritzsche, H., Müller, V., Rau, T., Schindlbeck, C., Rack, B., Janni, W., Coith, C., Beck, K., Jänicke, F., Jackson, S., Gornet, T., Cristofanilli, M., and Pantel, K., "Detection of circulating tumor cells in peripheral blood of patients with metastatic breast cancer: A validation study of the cell search system," *Clin. Cancer Res.* **13**, 920–928 (2007).
- Sarioglu, A. F., Aceto, N., Kojic, N., Donaldson, M. C., Zeinali, M., Hamza, B., Engstrom, A., Zhu, H., Sundaresan, T. K., Miyamoto, D. T., Luo, X., Bardia, A., Wittner, B. S., Ramaswamy, S., Shioda, T., Ting, D. T., Stott, S. L., Kapur, R., Maheswaran, S., Haber, D. A., and Toner, M., "A microfluidic device for label-free, physical capture of circulating tumor cell clusters," *Nat. Methods* **12**, 685 (2015).

- Scher, H. I., Heller, G., Molina, A., Attard, G., Danila, D. C., Jia, X., Peng, W., Sandhu, S. K., Olmos, D., Riisnaes, R., McCormack, R., Burzykowski, T., Kheoh, T., Fleisher, M., Buyse, M., and Bono, J. S., "Circulating tumor cell biomarker panel as an individual level surrogate for survival in metastatic castration-resistant prostate cancer," *J. Clin. Oncol.* **33**, 1348–1355 (2015).
- Song, Y., Zhu, Z., An, Y., Zhang, W., Zhang, H., Liu, D., Yu, C., Duan, W., and Yang, C. J., "Selection of DNA aptamers against epithelial cell adhesion molecule for cancer cell imaging and circulating tumor cell capture," *Anal. Chem.* **85**(8), 4141–4149 (2013).
- Umezawa, K. and Nuri, Y., "Progress of filtration technologies for inclusion removal," *Tetsu To Hagane* **75**, 1829–1838 (1989).
- Wasniewski, M., Guiot, A. L., Schereffer, J. L., Tribout, L., Mähär, K., and Cliquet, F., "Evaluation of an ELISA to detect rabies antibodies in orally vaccinated foxes and raccoon dogs sampled in the field," *J. Virol. Methods* **187**, 264–270 (2013).
- Went, P. T., Lugli, A., Meier, S., Bundi, M., Mirlacher, M., Sauter, G., and Dirnhofer, S., "Frequent EpCam protein expression in human carcinomas," *Hum. Pathol.* **35**, 122–128 (2004).
- Wu, L., Zamay, G. S., Kolovskaya, O. S., Zamay, T. N., and Berezovski, M. V., "Aptamer-based microfluidics for isolation, release and analysis of circulating tumor cells," *Trends Anal. Chem.* **117**, 69–77 (2019).
- Zhou, J., Mukherjee, P., Gao, H., Luan, Q., and Papautsky, I., "Label-free microfluidic sorting of microparticles," *Appl. Phys. Lett. Bioeng.* **3**, 041504 (2019).